Effect of process parameters of Plain Water Jet on the cleaning quality, surface and material integrity of Inconel 718 milled by Abrasive Water Jet

Lorena Cano Salinas, Xavier Sourd, Kamel Moussaoui, Sabine Le Roux, Mehdi Salem, Anis Hor, Redouane Zitoune

Effect of process parameters of Plain Water Jet on the cleaning quality, surface and material integrity of Inconel 718 milled by Abrasive Water Jet

L. Cano-Salinas [a], X. Sourd [a], K. Moussaoui [a], S. Le Roux [b], M. Salem [b], A. Hor [a], R. Zitoune [a,*]

[a] Institut Clément Ader, CNRS UMR 5312, 3 Rue Caroline Aigle, 31400 Toulouse, France
[b] Institut Clément Ader, CNRS UMR 5312, Campus Jarlard, 81013 Albi, France

A B S T R A C T

Abrasive Water Jet (AWJ) is considered as a promising milling method for difficult-to-machine aeronautical materials as Inconel alloy 718 (IN718). However, grit embedment during AWJ is known as a detrimental effect on certain applications as aircraft repair, where surface condition may play an important role on additive material technologies. To overcome this problem, Plain Water Jet (PWJ) has been used in the present study as cleaning process and demonstrated to be an effective method to remove grit particles from the surface with marginal alterations of surface state. In this paper, firstly the influence of AWJ process parameters on abrasive embedment and surface texture on IN718 specimens milled by AWJ were addressed. Then these surfaces were subjected to PWJ cleaning process and were extensively characterized in terms of grit embedment, surface texture and roughness, erosion depth, microhardness and residual stresses. Before cleaning, the milled surfaces presented a grit embedment level varying between 7 % and 14 %. One setting condition was selected for performing PWJ cleaning which reduced the grit level up to a quarter of the initial total surface area (less than 4 % in all cleaned surfaces) without relatively modifying neither the surface texture nor the erosion depth. Comparable microhardness gradients were observed before and after PWJ cleaning which corresponded to ~ 30 % higher than the bulk values at surface and then decreased beneath the surface up to *200 μm* before to reach bulk value (~ *245 HV*). Compressive residual stress state at surface initially induced by AWJ milling in some surfaces remained unchanged after PWJ process but in other ones was slightly relieved (~ *50 MPa*). Residual stresses after PWJ process resulted from − *630 MPa* to – *315 MPa* depending on the milling process parameters.

Nomenclature and abbreviations

AWJ	Abrasive Water Jet.
BSE	Back-scattered electron.
EDS	Energy-dispersive spectroscopy.
f	Traverse speed.
IN718	Inconel 718.
P	Pressure.
PWJ	Plain Water Jet.
Sa	3D roughness.
Sal	Autocorrelation length.
Sdr	Developed interfacial area ratio.
SE	Secondary electron.
SEM	Scanning electron microscopy.
SOD	Stand-off distance.
STD	Step-over distance.
Str	Texture-aspect ratio.
XRD	X-ray diffraction.

1. Introduction

Abrasive Water Jet (AWJ) technology for milling has found application in a wide range of sectors as the challenging aerospace industry. AWJ belongs to non-conventional machining process in which abrasive particles are mixed into a water jet entrained by high-pressures converted into high-velocities using a narrow nozzle (often *Ø 0.76–1.50 mm*) to erode the material when impacting onto the surface [1]. AWJ milling has been gaining use over conventional machining processes (*e.g.* milling and grinding) because it offers several advantages. AWJ has been shown to be suitable for removing material of complex geometry components as thin-curved blades because it keeps a constant thickness of material removal among the surface where conventional milling may

* Corresponding author.
E-mail address: redouane.zitoune@iut-tlse3.fr (R. Zitoune).

not be quite appropriated. Since material is removed by erosion, AWJ milling induces a marginal thermal damage on workpiece as well as it is suitable for processing hard-to-machine materials as nickel-based aerospace superalloys, *e.g.* Inconel 718 [2].

Beyond these advantages, an issue widely acknowledged in the AWJ process is the residual abrasive particles which embedded mechanically at surface during milling [3–7]. These abrasive particles may be act as fatigue crack initiators [2,3,8], detrimental condition for a finished surface or for subsequent processes in repair application of damaged aircraft engine components where 3D additive manufacturing (AM) technology is deposited [9]. In metallic materials, it has been reported up to 40 % of the total area of a milled surface consisted of grit embedment, and in the best cases, 5 %, depending on machining conditions [3,5–7,10].

Since AWJ process is characterized by a large number of machining parameters, researchers have attempted to reduce the levels of grit embedment by varying the process parameters. However, the scientific publications regarding metallic materials are limited. Traverse jet speed (*m/min*), jet impingement angle (°), distance between jet passes (step-over distance, *mm*) or grit size (mesh #) have been reported as adjustable parameters that can influence the level of grit embedment. Rivero et al. [3] studied abrasive embedment in alloy 718 surfaces milled by varying different AWJ process parameters. It was reported that grit embedment increased with increasing jet pressure, traverse speed and stand-off distance with step-over distance; whilst, an optimum higher level of grit embedment of 20 % was reported to occur at *0.3 grmin* of abrasive flow rate, whereas for *0.15* and *0.45 gr/min* the grit embedment was of ~ 14 %. Arola et al. [7] reported that abrasive embedment increased with increasing pressure and smaller abrasive particles in titanium surfaces. Boud et al. [4] examined #80 mesh garnet abrasive from five different sources when through-cutting titanium alloy by AWJ and concluded that, despite the different morphology, crushing strength and hardness of each abrasive type, there was no significant difference in the grit embedment level. Shipway et al. [6] examined two sizes of garnet abrasives particles by varying the jet impingement angles when milling titanium alloy surfaces. They observed that, for both abrasive sizes (#80, #200), the grit embedment increased with increasing the impingement angle due to the higher impulse during impact as the impingement angle was raised. Fowler et al. [5] investigated the effect of traverse speed, grit size, milling direction and jet impingement angle on the level of abrasive embedment in titanium alloy surfaces milled by AWJ and reported that for the two studied abrasive sizes (#80, #200) with a constant traverse speed of *0.18 m/min*, the forward milling resulted in high levels of grit embedment whilst backward milling resulted in lower levels of grit embedment for all impingement angles of 30°, 60° and 90°. However, for a higher traverse speed (*9.96 m/min*) they reported that the two modes of milling had no strong influence on grit embedment. Patel [11] compared straight and oscillation cutting techniques in AWJ with respect to grit embedment, and they found that for ductile materials, nozzle oscillation reduced by up to five times the abrasive embedment in surface compared with a straight cutting.

On the other side, in order to remove contaminants from the surfaces, several cleaning methods have been reported in the literature. Mechanical or chemical cleaning processes are often used for removing metallic contamination, tarnish and oxidation resulting from hot working or heat treatments of nickel-base superalloy components [12]. Mechanical cleaning methods include dry or wet abrasive blasting, polishing (with ceramic materials) and wet tumbling. Chemical methods are more used than mechanical means, namely: picking and vapor degreasing or alkaline cleaning followed by either water rinsing or soaking. The applicability of these methods is determined by the shape of the component, the surface finish requirements and the allowable metal loss, however, a combination of two or more methods are often necessary. Such methods may require rigorous inspections to prevent over-etched parts or excessive metal surface roughening; even hydrogen embrittlement, which it is not commonly to occur in super-alloys but are not immune to it [12]. Another popular cleaning method is the ultrasonic. Ultrasonic cleaning can remove strongly embedded contaminants from parts immersed in aqueous medium by using high-frequency sound waves in the range between 40 and 200 kHz. The ultrasonic energy is applied to the cleaning solution (water, various forms of alcohol, degreasing, acids, *etc.*) causing cavitation to scrub the surface free of pollutants [13]. However, this method requires a rigorous selection of frequency and amplitude of sound waves due to the tendency of the ultrasonic energy to damage parts. Furthermore, this cleaning method involves a rise in cost due to the tank filled with cleaning agents.

On the other hand, abrasive-less water jet, commonly called Plain Water Jet (PWJ), is recently reported in the literature as a surface treatment – for improving fatigue strength by introducing compressive residual stresses, for medical applications where an increase in surface roughness is required [7,14–17] – or cleaning method, – *e.g.* for removing oxygen layer in titanium alloys surfaces usually formed after service at elevated temperatures [18].

However, the use of Plain Water Jet method for addressing the problem of grit embedment induced by AWJ milling is until today scarcely studied in the literature [3,10,15]. Moreover, there is a knowledge gap in the literature concerning surface integrity aspects after PWJ cleaning method (surface quality, material thickness removed, residual stresses, hardness, *etc.*). Rivero et al. [3] applied PWJ process to release the surface of embedded abrasives due to AWJ milling from alloy 718 surfaces. They demonstrated that all the embedded abrasive particles were removed under pressures between *160* and *360 MPa*, traverse speeds ranging *0.1–0.9 m/min*, stand-off distances varying *10–90 mm* and from one to four jet passes. Further, they observed that, in several PWJ conditions, the roughness produced by AWJ was reduced by the cleaning operation between 2.5 % and 40 % because of water droplets eroded the peaks and valleys produced by abrasive particles impact. Nevertheless, the material removal induced by PWJ was not quantified in this study, which is the utmost importance for aeroengine components as thin-curved blades. Huang et al. [15] studied AWJ milling for the removal of alpha case from titanium alloys followed by PWJ to remove the grit embedment. They have tested several experimental conditions for PWJ to evaluate the efficiency of grit removal. In the conditions performed in their study, it was found that there was better performance to remove the grit embedment from 20 % to 6–10 % when using *SOD* between *30–50 mm* and for jet impingement angle of 90°. Besides, when using traverse speeds of *0.5* and *1.5 mm/min* as well as when increasing the number of jet passes, the grit embedment reduced from 29.8 % to less of 10 %. Further, they observed higher grit removal effectiveness with a PWJ scanning path in a feed direction perpendicular to that used for the AWJ milling. Arola et al. [16] reported that in titanium alloy residual stresses resulting from PWJ increased with abrasive size and jet pressure. Lieblich et al. [14] reported that higher waterjet pressures in titanium alloy did not induce higher residual stresses, but only increased material erosion. They explained that higher amount of removed material allows a partial relief of residual stress in spite of the higher impact energy. Azhari et al. [17] investigated the influence of PWJ in stainless steel and reported that compressive residual stresses, hardness and roughness increased with higher number of passes, however, they suggested that higher levels of roughness may affect the fatigue strength, due to the tendency of crack initiation. Holmberg et al. [19] evaluated the performance of high-pressure Plain Water Jet (*360 MPa*) in an Inconel 718 shaft to remove electrical discharge machining (EDM) residue by using only one processing condition, which resulted in a removed layer of *39.1 μm*. Further, the authors indicated a surface roughness of *3.5 μm* and compressive residual stresses with a peak of *750 MPa* at ~ *7 μm* beneath the surface that decreased along a depth of ~ *150 μm*.

There is a lack in the literature providing an extensive analysis of surface state (topographical and mechanical aspects) in Inconel 718 before and after PWJ process with prior AWJ milling. It could be very interesting to estimate the relevance and the effectiveness of the

combination of the AWJ milling followed by PWJ process in alloy 718, for a multi perspective application: as milling operation for difficult-to-machine materials as Inconel 718 where a determined surface quality is desired, and also as a precedent step to the repair application where removal of damaged zone is required; in both cases a state free of abrasive residues is well preferred.

The purpose of the present investigation is, in a first stage, to quantify grit embedment and to characterize the surface in terms of texture of Inconel 718 surfaces milled by AWJ process. To achieve this objective, AWJ milled surfaces at different process parameters (*viz.* jet pressure, traverse speed and step-over distance) were taken from a previous study [20] and then the surfaces were subjected to PWJ cleaning process in order to remove the grit embedment by using a set of processing parameters by considering a trade-off among the removed grit and material erosion depth. After cleaning, the influence of Plain Water Jet (PWJ) process on grit embedment removal, the modifications in surface texture and roughness (by using *Sa*, *Str*, *Sal* and *Sdr* parameters), the thickness of removed material, the microhardness and the residual stresses were examined.

2. Experimental procedure

2.1. Equipment and material

AWJ and PWJ processes were conducted on a Flow MACH4-C Waterjet Machine. The cutting head of the machine is composed of an orifice diameter of *0.33 mm*, a focusing tube length of *76 mm* and a nozzle diameter of *1.016 mm*. All tests for AWJ and PWJ were performed at a jet impingement angle to 90° (cutting nozzle perpendicular to the cutting direction) with the nozzle in air. The overall view of the experimental setup is shown in Fig. 1.

Annealed commercially Inconel alloy 718 was utilized in this investigation. Inconel 718 was provided in plate form with *3.71 mm* thickness. Test samples were prepared in rectangular form of *180 mm* × *20 mm* by AWJ cutting. The chemical composition of this alloy is given in Table 1. The hardness of the bulk material is 245 ± 15 *HV* measured as indicated in 2.4.

2.2. AWJ milling

Abrasive garnet (Wuxi Ding Long Minerals Co., Ltd) mesh #120 was employed for AWJ milling operation. For economical reasons, the abrasive size as well as the abrasive flow rate were kept fixed in this study (Table 2). A *STD* value of *100 mm* was used to make possible the milling of workpieces with complex shapes as large curvatures. Full factorial tests, corresponding to three levels of jet pressure (*P*), traverse speed (*f*) and step-over distance (*STD*), as stated in Table 2, were performed resulting in twenty-seven different experimental conditions similar to those used in previous work [20].

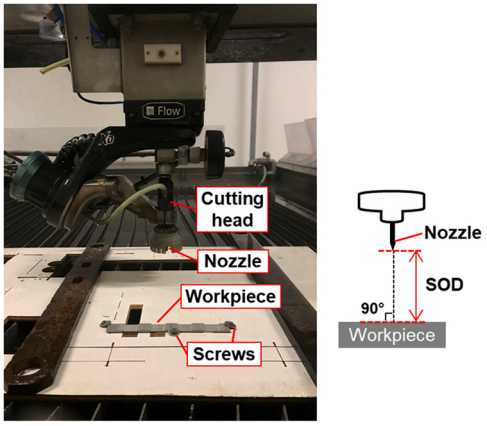

Fig. 1. Experimental setup for AWJ and PWJ processes with a schematic showing the *SOD* process parameter and the impingement angle between the nozzle and the sample.

Each specimen was milled by creating four "blind" pockets of *20 mm* of length spaced *20 mm* apart. These four pockets in each specimen were machined with identical milling parameters in order to ensure a good repeatability of the AWJ process. All pockets were milled following a raster scan tool strategy by keeping jet direction changes outside of the workpiece (Fig. 2).

2.3. PWJ cleaning

Over the "blind" pockets created by AWJ milling, Plain Water Jet (PWJ) post-processing was performed without abrasive particles in an attempt to remove embedded abrasive particles. Similar tool path and feed direction to those used for AWJ milling were employed for PWJ cleaning process.

Before cleaning of pockets, preliminary tests were performed in order to identify a proper set of PWJ parameters allowing to preserve the topographies of the milled pockets (both in terms of depth and surface roughness and texture) as well as their mechanical state (hardness and residual stresses). Thus, the set of parameters selected to perform the PWJ cleaning process (Section 3.2.1) in AWJ milled surfaces was fixed at: $P = 200$ *MPa*, $SOD = 50$ *mm*, $STD = 0.5$ *mm*, and $f = 1.0$ *m/min*. Water jet pressure of *200 MPa* was selected because showed a good effectiveness to remove embedded abrasive particles with a minimal thickness of removed material. Stand-off distance was fixed at *50 mm* according to Rivero et al. [3] who efficiently performed PWJ cleaning tests using a *SOD* between *10–90 mm*. Initially, a $SOD = 100$ *mm* as to this used for AWJ milling was attempted to be used for PWJ cleaning but such value showed almost not efficient to remove grit, thus, in order to keep a relatively large value *SOD* for machining components with significant curvature, a value of $SOD = 50$ *mm* was selected. $STD = 0.5$ *mm* was selected in an attempt to improve cleanliness by increasing the overlap of the water jet passes in surface.

Among the twenty-seven milled specimens, only seven samples were selected to perform the PWJ cleaning in order to simplify the analysis, and from these seven specimens only the pockets number 3 and 4 were cleaned. Thus, three distinct degrees of texture (low, medium and high) produced by AWJ milling were selected from the evaluation of the texture-aspect ratio (*Str* parameter defined in Section 2.4). These selected specimens are: two specimens milled at $P = 200$ *MPa* chosen as isotropic textures, three specimens milled at $P = 250$ *MPa* as middle surface texture, and two specimens milled at $P = 300$ *MPa* as anisotropic surfaces in order to study different specimens of each different pressure used for AWJ milling.

2.4. Surface characterization techniques and procedures

The 3D surface topographies of the milled and cleaned pockets were measured by means of Alicona Infinite Focus 3D optical profilometer. From these surface mappings, the surface topography over an area of *5.7* × *5.7 mm* at the center of the pocket as well as the thickness of material removal along *40 mm*-long and *2 mm*-wide, were measured following the experimental procedure fully described in previous work [20]. The scanning locations of the pocket measurements are shown in Fig. 3a.

The topography data were treated by means of AltiMap software. Surface topography was characterized using height, spatial and hybrid parameters according to the ISO 25178-2 standard. Such mentioned parameters have been used in previous works [21–23] to characterize topographical properties of surfaces. The parameters used in this study were *Sa*, *Str*, *Sal* and *Sdr*. The arithmetic mean height parameter (*Sa*), is commonly used to characterize surface roughness without regard of the direction by quantifying the average absolute height of peaks and valleys of interest [21]. As a complement to height parameter *Sa*,

Table 1
Chemical composition of the wrought Inconel 718 material.

Ni (%)	Cr (%)	Fe (%)	Nb (%)	Mo (%)	Ti (%)	Al (%)	Co (%)	C (%)	Mn (%)	Si (%)	S (%)	P (%)	B (%)	Cu (%)	Ta (%)
53.47	18.28	18.2	5.06	2.98	0.96	0.51	0.17	0.03	0.09	0.08	0.0003	0.007	0.001	0.06	0.01

Table 2
Parameter setting for AWJ process.

	Levels for AWJ		
Variable parameters			
Pressure (*P*), MPa	200	250	300
Traverse speed (*f*), m/min	0.5	1.0	1.5
Step-over distance (*STD*), mm	0.5	1.0	1.5
Fixed parameters			
Stand-off distance (*SOD*), mm	100		
Abrasive flow rate, kg/min	0.18		
Abrasive size	#120		

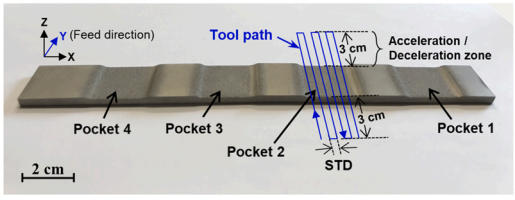

Fig. 2. Overview of the specimen machined by AWJ at $P = 300\ MPa$, $f = 1\ m/min$ and $STD = 1\ mm$ showing milled pockets and the tool path.

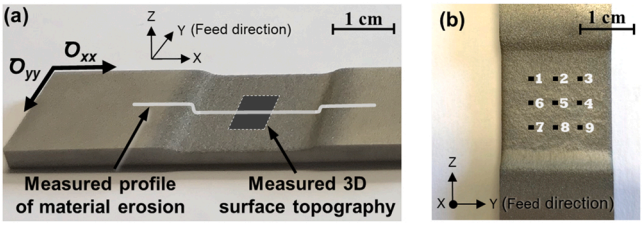

Fig. 3. Location of pocket measurements (a) for the surface topography over an area of $5.7 \times 5.7\ mm$ and the profile of material removed thickness of $40\ mm$-long $\times$ $2\ mm$-wide, and (b) for the grit embedment over on nine different zones of an area of $850 \times 734\ \mu m$ each.

information describing the texture is given by *Str* and *Sal* spatial parameters and *Sdr* hybrid parameter. Spatial parameters are used to further describe the texture and orientation of a surface with respect to a whole image [21]. The texture aspect ratio parameter (*Str*), is an evaluation of the surface texture isotropy. *Str* is a unit-less parameter and is denoted from 0 to 1 (or expressed as percentage between 0% and 100%) [24]. An isotropic texture has the same properties regardless of the direction, whilst an anisotropic surface has a dominant texture direction [24]. $Str < 0.3$ represents an anisotropic texture, whilst $Str > 0.5$ describes an isotropic texture [21]. The autocorrelation length (*Sal*), provides information about the finesses of a surface, the smaller the *Sal* value, the finer the features [21]. *Sal* parameter is defined as the horizontal distance of the autocorrelation function (ACF) which has the fastest decay to a specific value ($s = 0.2$) [24]. For an anisotropic surface, *Sal* is in the direction perpendicular to the surface lay [24]. Further, the developed interfacial area ratio (*Sdr*), is used as a measure of the surface complexity, it is typically described in percentage. A perfectly flat and smooth surface would have $Sdr = 0\ \%$ [24].

Surfaces were also observed using FEI Nova NanoSEM 450 Scanning Electron Microscope (SEM) with Back-Scattered Electron (BSE), secondary electron (SE) and Energy-dispersive spectroscopy (EDS) detectors. Before and after cleaning, nine micrographs ($850 \times 734\ \mu m$ each image field) were taken at different position locations (Fig. 3b) on the pocket number 3 of all specimens. These micrographs were then post-treated with image analysis by means of ImageJ software by using a gaussian filter to reduce image noise and to enable detection of abrasive particles boundaries. Then, a suitable threshold was applied to identify the darkest zones corresponding to abrasive particles (image binarization), as illustrated in Fig. 4. To quantify the level of grit embedment, the surface area corresponding to abrasive particles was determined from the total area per image field and converted into a percentage. The grit embedment percentage is the average of the nine different measurements per pocket with its standard deviation (pocket 3 of all specimens).

Granulometry and shape factor of abrasive grit were studied in order to better understand the effectiveness of grit removal on the AWJ milled surfaces. A MasterSizer 3000 instrument from Malvern Panalytical was used for the granulometric analyses. This apparatus is based on the theory of laser diffraction (Mie or Fraunhofer theory). This relates the angle of the laser beam with the particle size. The quantity of the sample for the analysis was *20 ml* of abrasive powder. The powder was feed into the apparatus and dispersed in an air stream at *3.5 bar* of pressure. The granulometry was analyzed from two different samples of abrasives: abrasive grit as provided and, abrasive debris collected of the machine's catch tank after usage for AWJ milling. Each abrasive powder sample was measured twice (*Measure A*, *Measure B*) in order to duplicate measurements of each sample. Normal distribution model was used to fit the data.

The initial shape of single abrasive particles was measured by using SEM. Fifteen micrographs were taken, then, from these micrographs, 230 grain particle shape were extracted with image analysis by using Aphelion software. Circularity and elongation shape factors (both range from 0 to 1), were obtained to characterize these 230 particles. For a perfect circular particle, the circularity is equal to 1; elongation index is zero for a circle and approaches 1 for a long and narrow ellipse.

Residual stress measurements were performed by X-ray diffraction (XRD) technique. Residual stresses were evaluated in the middle of the machined pocket across and along (σ_{xx}, σ_{yy}) the feed direction (Fig. 3a). The XRD measurements were performed using 6-axis XRayBot® apparatus equipped with a goniometer with a pure Si solid detector and Mn radiation source (Mn-Kα1, $\lambda = 2.10$ Å). Setting parameters and computation data used are similar to those described in previous work [20].

Once the surface characterizations were completed, only two specimens, of the seven selected to be cleaned, were chosen to analyze the effect of the PWJ cleaning operation on the sub-surface hardness and for observations of grit removal in cross section. It was selected two specimens milled at two different pressures, both with different traverse speed and *STD*. The two selected specimens were those milled at $P = 250\ MPa$, $f = 1\ m/min$, $STD = 0.5\ mm$ and $P = 300\ MPa$, $f = 0.5\ m/min$, $STD = 1.5\ mm$. The cross sections of the pockets number 1 (uncleaned) and number 4 (cleaned) of these two specimens were cut on the middle of the pocket in two orientations: parallel and perpendicular to the feed direction (Fig. 5). In addition, one cross-section was cut of wrought material as provided in order to measure its microhardness. All cross-sections were prepared by grinding with different grit sizes of SiC paper (from P400 to P4000) and then by polishing with diamond powder to mirror-finished. The sub-surface microhardness measurements were performed using a microhardness testing MICROMET 5104 (from Buehler GmbH) driven by Omnimet MHT software according to the ISO 6507-1 standard. Vickers indenter was utilized to penetrate the

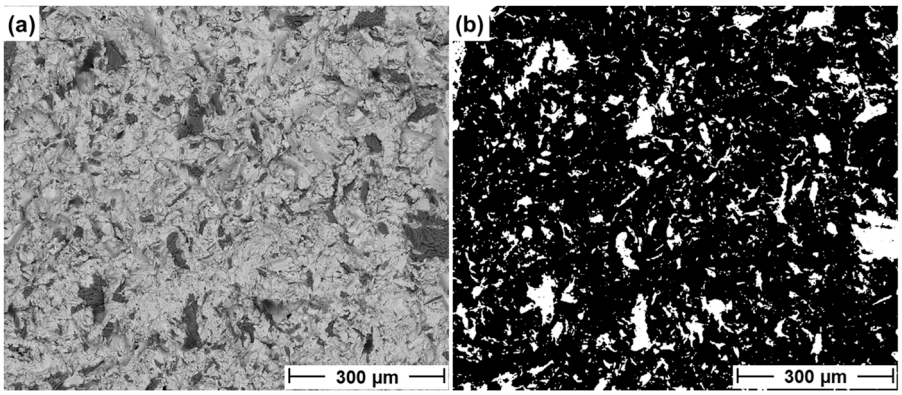

Fig. 4. (a) SEM micrograph of abrasives embedded at surface after AWJ milling at $P = 300\ MPa$, $f = 0.5\ m/min$ and $STD = 1.5\ mm$ with its (b) image binarization showing the grit in white color and black background corresponding to Inconel 718 material.

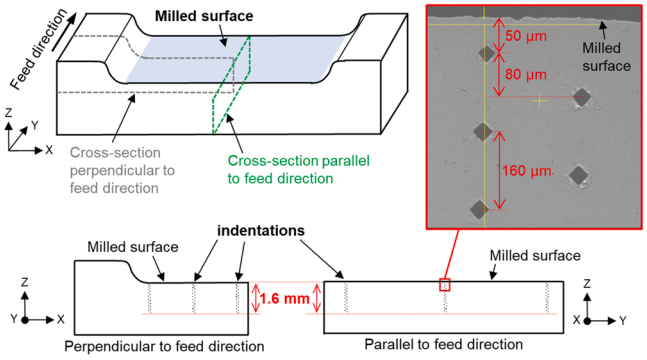

Fig. 5. Schematic showing micro-indentations in the cross-sections of a milled pocket for microhardness measurements.

polished surfaces with a load of *200 gf* applied during *10 s*. In each cross-sectional, three columns of 20 indentations in zigzag pattern were made toward the sub-surface, and an average of the sixty measured values was considered as the microhardness for each direction. The first row of indentations was located around *50 µm* below the milled surface. Indentations, separated from each other in *80 µm*, were performed up to *1.6 mm* in-depth (Fig. 5). For the cross-sectional of the bulk sample, the procedure was identical to the milled cross-sections except for the number of indentations per column, where each filiation of 46 indentations were performed throughout the thickness of the plate.

3. Results and discussion

3.1. AWJ milling

Due to the limited thickness of material plate (*3.71 mm*), two specimens were shattered when milling at *250 MPa* and *300 MPa* of pressure both with traverse speed of *0.5 m/min* and step-over distance of *0.5 mm*. Thus, only twenty-five testing conditions could be analyzed in the present work.

3.1.1. Qualitative observation of milled surfaces

Examination of micrographs of IN718 surfaces milled by AWJ reveals that all the surfaces present embedded abrasive particles (Fig. 6); most of these particles being less than *50 µm* in size. Since this size is much smaller than the original size (*180 µm*) of the abrasive (*i.e.* as received state) employed to mill the surfaces (Fig. 7b), it may be assumed that only fragments of original particles are embedded. This is because upon the jet impact on the surface, the abrasive particles can break into smaller portions [5]. This can be verified by comparing the micrographs of the abrasive (as supplied) with the debris (after milling) respectively in Fig. 7a,c which clearly show that the abrasives break into very small portions either by impact on the surface and/or by collisions among the particles with the accelerated water in the mixing tube of the machine [1].

In Fig. 7b it can be observed that the abrasive garnet has not an homogeneous grain size, showing a 15 % in volume weight of abrasives with a size of *180 µm*, while debris of abrasives after milling (Fig. 7c) show a large dispersion in size, most of these particles are nanometric sized, corresponding only 7 % of debris to *87 µm* in size (Fig. 7d).

Further, Fig. 6b reveals two types of embedded abrasive particles: oxides and organic particles. From a performed analysis by energy dispersive X-ray spectroscopy (EDS) as shows Fig. 8b, the main oxide particles embedded are silica (SiO_2), which are the mainly constituent of the abrasive medium, followed by aluminum oxide (Al_2O_3), ferric oxide (Fe_2O_3) and magnesium oxide (MgO). Such chemical compositions of embedded particles were compared with those of the abrasive grit as received, and presented identical constituents (Fig. 8a), which corroborates that the dark zones in SEM micrographs correspond well to embedded grit. The superficial darkest zones (Fig. 6b) correspond to organic particles which could be carbon, oxygen or hydrogen. These organics can be removed more easily (*e.g.* by rinsing with acetone). However, oxide pollutants need be removed by a cleaning process because the embedment behavior difficult the ability to be removed [15].

On the other side, SEM micrographs analysis reveals that the material removal of Inconel 718 is mainly produced by micro-cutting mechanism observed in form of plastic deformation induced by the impact of the abrasive particles on the target material (Fig. 9a–b). Repeated impacts by high-velocity particles induce deep craters and lip formations. Further, abrasive particle shape has an important influence on the erosion mechanism. Generally, the more sharp-edges abrasive grains, the greater the erosion [1]. Thus, material removal mechanism due to cutting-deformation is dominated by angular abrasive particles, whereas, the plowing deformation is significant for spherical particles [1]. In the micrographs of Fig. 9 is evident that micro-cutting due to plowing deformation is the predominant removal mechanism in IN718, which relates ductile behavior of the material. Further, Fig. 9c shows two types of crater formation: one due to an angular abrasive particle and the other owing to a rounded particle. Results about shape factor of single abrasive particles of garnet (Table 3) confirm a high index of circularity of particles (*0.71*), which is consistent with the plowing deformation mechanism mostly observed in the micrographs.

The images of Fig. 10**a** show different grain shapes for the garnet abrasive used in this study, namely spherical and sharp-edges particles. Moreover, in the field of erosion, it was reported that shape factor as well as the particle-hardness may have an influence on material removal. Angular and hard abrasive grains improve the material-

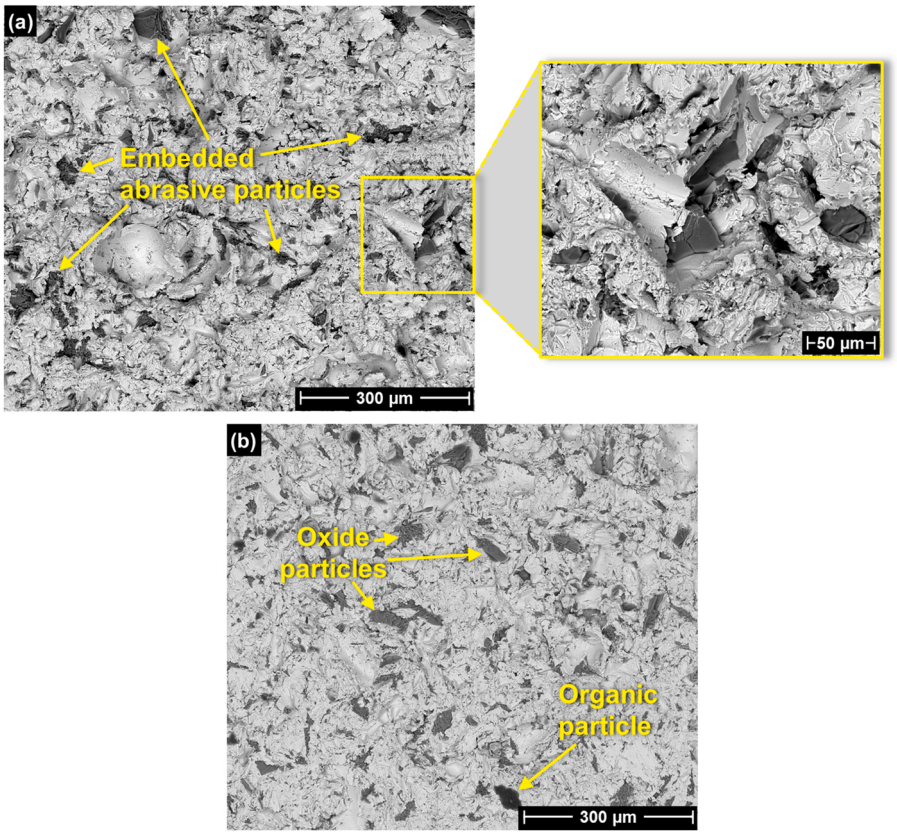

Fig. 6. SEM micrographs of IN718 milled surfaces by AWJ showing (a) the embedded abrasive particles in × 150 magnification with a zoomed view of grit embedment in × 500 magnification ($P = 300$ *MPa*, $f = 1.5$ *m/min* and $STD = 1$ *mm*); (b) different types of embedded abrasive particles in × 150 magnification ($P = 200$ *MPa*, $f = 1$ *m/min* and $STD = 0.5$ *mm*).

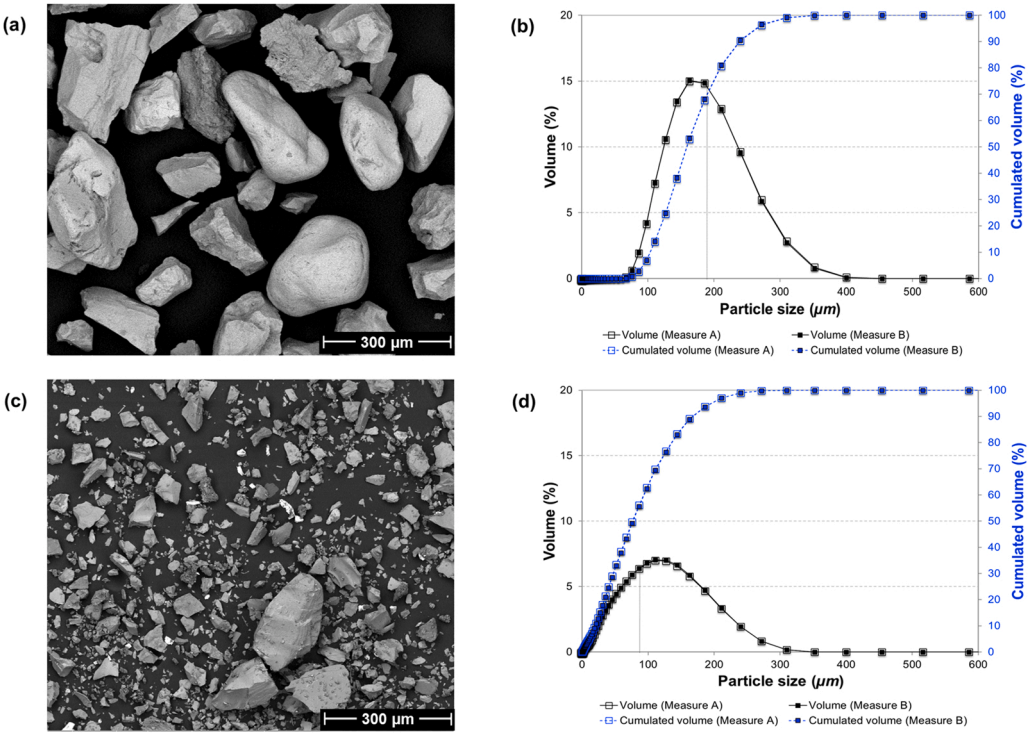

Fig. 7. SEM micrographs in × 130 magnification of the morphologies of (a) the garnet grit #120 before employ for AWJ milling and (c) the grit debris after AWJ milling; and graphs of abrasive size distribution measured by laser diffraction spectroscopy (b) before AWJ milling and (d) after AWJ milling.

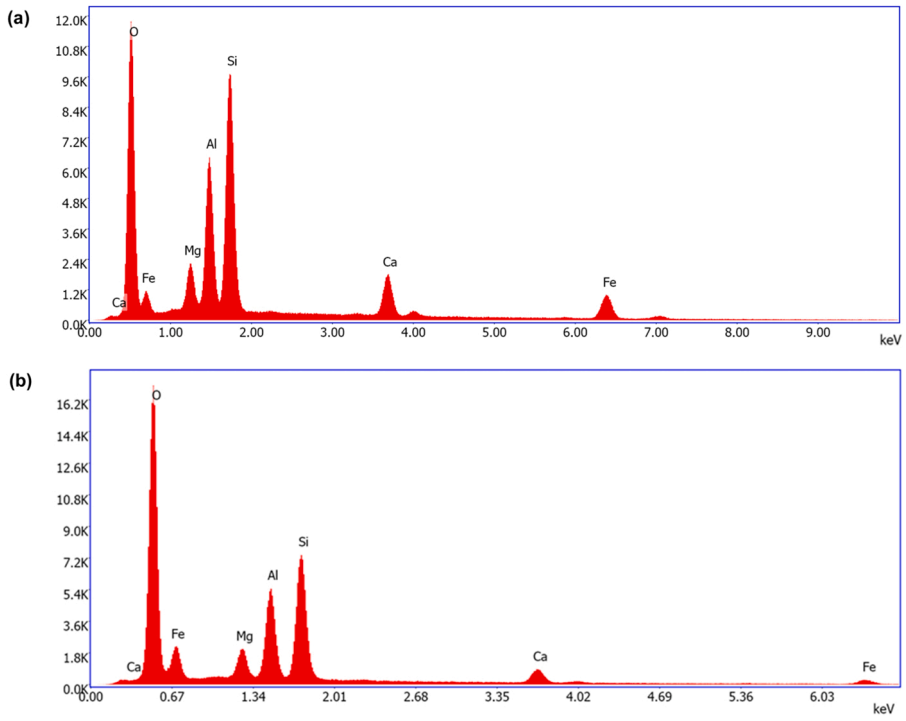

Fig. 8. EDS spectrum showing the chemical analysis of (a) the abrasive garnet grit as received state and (b) the embedded grit in surfaces after AWJ milling process.

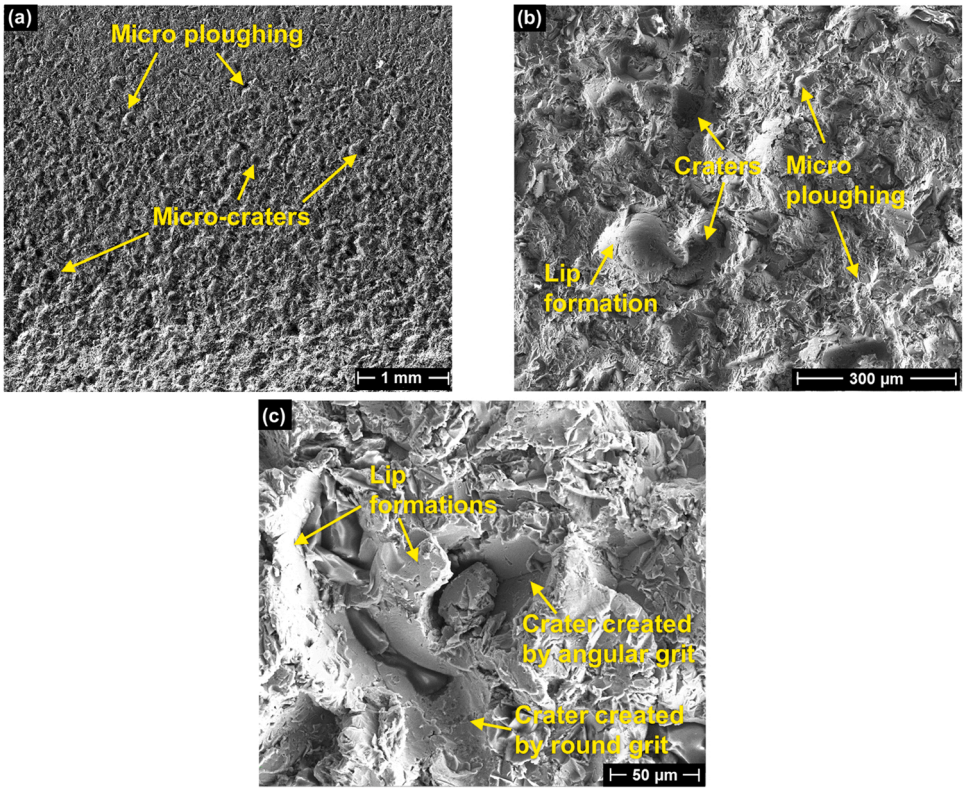

Fig. 9. SE morphologies of samples milled at (a) $P = 300\ MPa$, $f = 0.5\ m/min$ and $STD = 1\ mm$ in $\times$ 25 magnification; (b) $P = 300\ MPa$, $f = 1.5\ m/min$ and $STD = 1\ mm$ $\times$ 150 magnification; (c) $P = 250\ MPa$, $f = 1\ m/min$ and $STD = 1.5\ mm$ in $\times$ 500 magnification.

removal process in ductile materials [1,25]. However, these topics are not part of the present study.

3.1.2. *Effect of AWJ milling parameters on surface texture*

The effect of process parameters on surface texture was examined from the surface topographies performed on AWJ milled pockets. Different textures were produced depending on the process parameters

Table 3
Mean values of shape factors indexes of garnet abrasive particles used for AWJ process.

Abrasive material	Sample size (grains)	Shape parameter			
		Circularity	st. dev	Elongation	st. dev
Garnet	230	0.71	0.15	0.40	0.22

(Fig. 11). Jet pressure could intensify surface texture by increasing the amount of kinetic energy of the jet on the target material. The effect of traverse speed on the surface texture can be observed in Fig. 11**b,d,f**. These textures correspond to the surfaces milled at *0.5, 1* and *1.5 m/min* respectively at the same pressure (*P)* and step-over distance (*STD*) parameters. As traverse speed increases, a less textured surface is produced. This is because a short time of a jet pass could not quite erode the surface.

Further, the surface texture also appears to be highly dependent on the step-over distance (*STD*) parameter. In order to illustrate this phenomenon, it is assumed that the distribution of the jet energy fits a Gaussian distribution (Fig. 12**)**. In this case, a low *STD* is more likely to produce a fine surface texture due to greater overlapping between jet passes (Fig. 12**a**). Conversely, a higher *STD* generates rougher surface topographies, allowing peak formations in the zones where the jet passes are not overlap enough (Fig. 12**b**). Similar results have been observed when milling of carbon fiber-reinforced polymer (FRP) by AWJ process [26]. However, *STD* and traverse speed parameters, both strongly influence the surface texture at the same time. High *STD* values combined with low traverse speeds, regardless of the pressure, present well-marked grooves (Fig. 11**c,e,g**) even observed at naked eye. These grooves follow the jet pass direction.

However, the topographies obtained after AWJ milling, as depicted in Fig. 11**,** showed that the preferential texture orientation expected from Fig. 12 (a "theoretical" process of a single process parameter: *STD*) does not correspond exactly to the experimentally obtained surfaces (which are more complex) because the texture and directionality of the surface could be influenced depending on the intensity of the three combined process parameters (*P*, *f*, and *STD*) and only areal parameters can integrate information in all directions. The texture aspect ratio (*Str*), is one of the most important parameters when characterizing a surface in an a real manner [24]. This spatial parameter (*Str*), is a numerical representation of the strength of orientation [21].

The texture-aspect ratio (*Str)* of the surfaces produced after AWJ milling ranges from *0.2* to *0.9* depending on the process parameters, meaning a variety of isotropic and anisotropic surfaces. The most textured surfaces, exhibiting the lower *Str* (< 0.3), were produced at high *STD* (*1.5 mm*) regardless of the jet pressure used (Fig. 11**c,e,g**). On the contrary, more isotropic textures ($Str > 0.5$) were generated when using low pressure (*200 MPa*) with $STD = 1$ *mm* for all traverse speeds (Fig. 11**b,d,f**). However, the analysis of texture needs the complement of other areal parameters to better describe the surface texture. *Sal* values are not smaller for reduced *STD* as expected because the interaction between the different AWJ process parameters, instead low *Sal* values described more isotropic textures surfaces where the grooves of *STD* were not significant (Fig. 11**d,f**). *Sdr* parameter indicates that the flattest or smoothest surface was that with $Sdr = 6$ % followed by the surface with $Sdr = 12$ % (Fig. 11**a,b).**

3.1.3. *Effect of AWJ milling parameters on grit embedment*

Fig. 13 shows the evolution of the surface fraction of grit embedment as a function of the jet pressure (*P*) and the step-over distance (*STD)* for the three different traverse speeds (*f*). Each point in these graphs represents an average value of nine measurements in the pocket number 3 where examination where performed for each specimen. The grit embedment ranges from 7 % to 14 % of the total surface area, depending on the AWJ process parameters. This is way lower than the grit embedment reported in [10] when milling Ti6Al4V by AWJ, which was around 40 % of the total surface area. This can be due to the machinability of the two materials. As Inconel 718 has a lower machinability than Ti6Al4V (12 % and 20 % respectively), it is more difficult for the abrasive grit to embed in the material.

The grit embedment seems to decrease as *P* increases as well as when decreasing *STD* and no clear effect was observed in function of the *f* parameter (Fig. 13**a–c**). In fact, if we refer to the literature review, during air jet blasting, the contamination rate increases with the increasing of the air pressure [27,28]. Indeed, in the work of Getu et al. [27], it was mentioned that, with an increase in the impact velocity of the grit, the grit penetration depth also increases [27]. However, when considering the Abrasive Water Jet process, the physics occurring for the particle embedment can be different compared to the air jet blasting. In fact, the impact velocity of the grit increases with an increase of the water jet pressure. In this case, it can be supposed that, with an increase in the water jet velocity (or pressure) some embedded grit can be removed from the machined surface due to the pressure forces locally applied by the water on the wall of the grit. In addition, in the work of Rivero et al. [3] on milling of IN718 material, it was observed that, the grit embedment remains stable when the pressure varies from *160 MPa* to *260 MPa*. Further, it was reported by the same authors the effect that traverse speed increased the grit embedment, in contrast, in the present study no significant effect for *f* parameter was observed. It is important to noticed that, in the work of Rivero et al. [3], all the experimental tests have been conducted with a stand-off distance inferior to the one used in the present work (which is of *100 mm*). In fact, when increasing the stand-off distance, the grit energy is reduced. Therefore, the influence of the traverse speed on grit embedment may be minor. The trend of a greater *STD* increased the grit embedment as depicted in Fig. 13 could be explained by the fact that smaller step-over distances lead to a larger overlapped area between different jet passes over the surface when

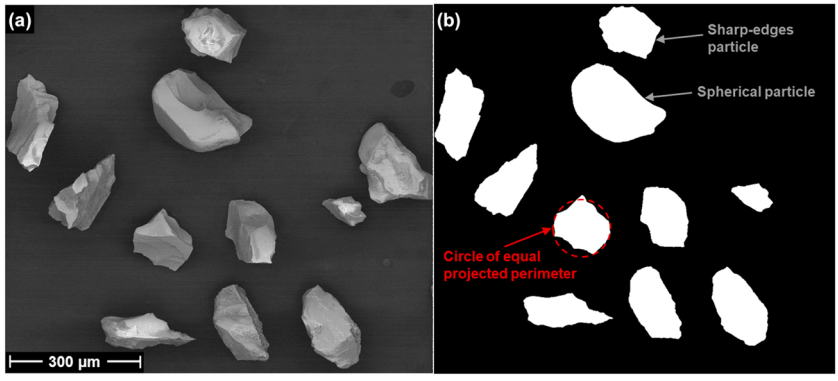

Fig. 10. (a) SEM micrograph of garnet abrasive grains with its (b) binary image showing different grain shapes and the circularity shape factor for a single particle.

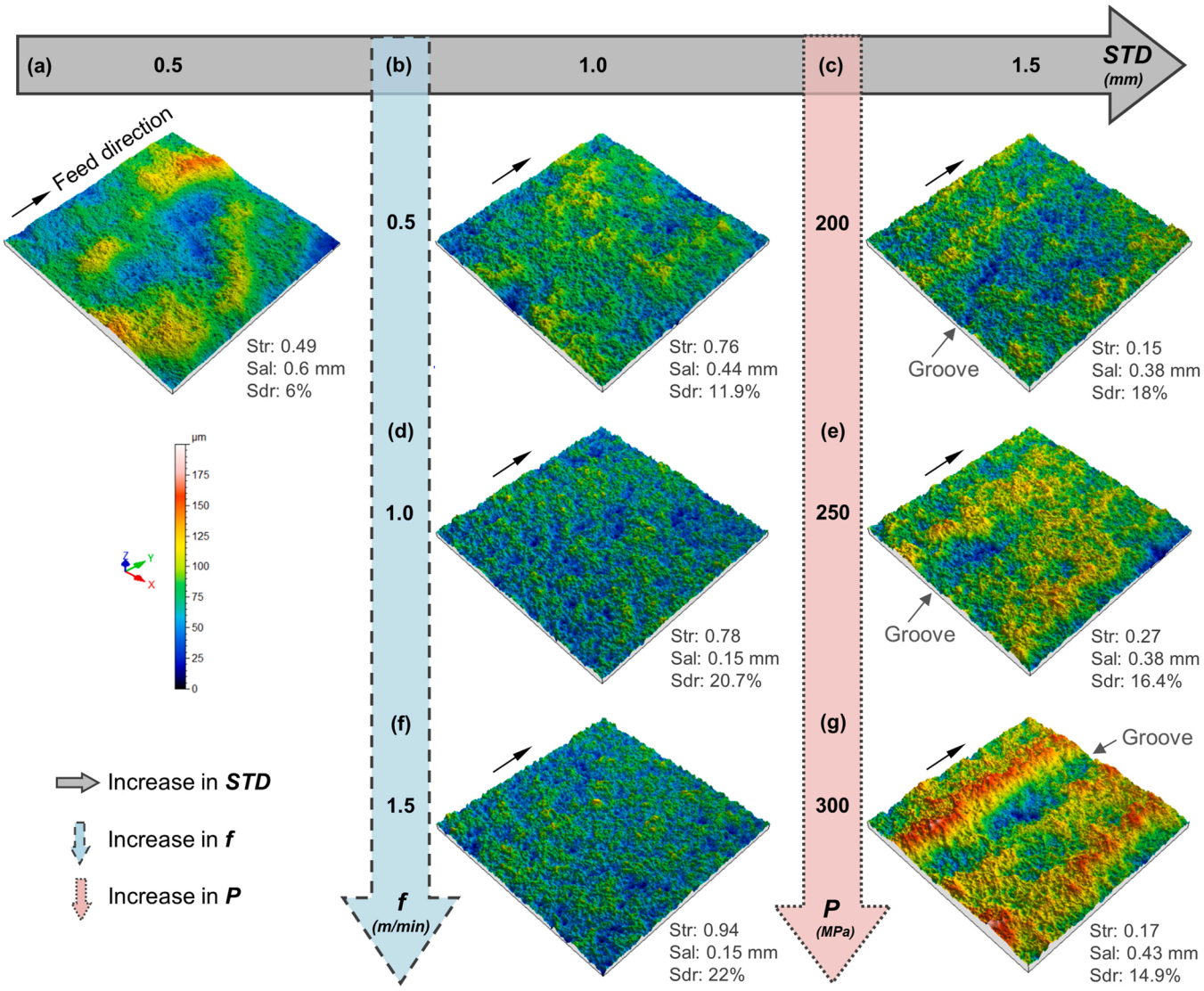

Fig. 11. Different IN718 surface textures of pocket 2 of specimens milled by AWJ at $P = 200$ *MPa* with constant $f = 0.5$ *m/min* and (a) $STD = 0.5$ *mm*, (b) $STD = 1$ *mm*, (c) $STD = 1.5$ *mm*; $P = 200$ *MPa* with constant $STD = 1$ *mm* and (d) $f = 1$ *m/min*, (f) $f = 1.5$ *mm*; and $f = 0.5$ *m/min* with constant $STD = 1.5$ *mm* and (e) *250 MPa*, (g) *300 MPa*. The little arrow indicates the feed direction. Each surface area is *5 mm* × *5 mm* in size.

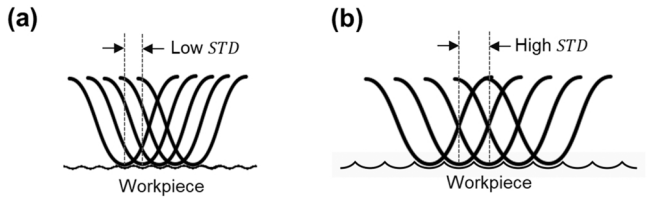

Fig. 12. Graphs describing the effect of the step-over distance (*STD*) parameter on surface textures produced by AWJ milling for (a) low *STD* and (b) high *STD*.

milling, which can remove embedded particles by subsequent jet passes.

3.2. PWJ cleaning process

3.2.1. Effect of PWJ cleaning post-process on surfaces milled by AWJ

PWJ cleaning process produced a significant reduction in the level of embedded abrasive particles in the surface of the seven specimens selected to be cleaned, as illustrated in Fig. 14.

The residual grit after PWJ cleaning process varied between 3 % and 4 % of the total milled surface regardless of the initial level of grit embedment produced by the AWJ (Fig. 15). This implies a reduction of embedded abrasives before and after PWJ cleaning from 4% to 11 % of the total surface area. The fact that the embedded particles were not completely removed could be explained by the existence of two types of embedded abrasive particles, namely deposited particles and submerged particles [3,15]. Thus, it is assumed that the water jet, at the cleaning parameters selected for the present study, could not remove some submerged particles, located in a crater and/or partially covered by material. In Fig. 16 is depicted in cross sectional the embedded abrasive particles before and after PWJ cleaning. Fig. 16**a,c** shows embedded grit after AWJ process where submerged abrasives partially covered by a layer of IN718 material were observed. After PWJ cleaning, Fig. 16**b, d** shows the residual grit in the narrow corners of the cavities, when the water jet was not able to completely dislodge the abrasive. Most of residual grit is less than *20 µm* and up nanometric size. This residual grit was analyzed in section by EDS and confirms the same chemical composition as that shown in Fig. 8**b**.

Before and after PWJ cleaning, the texture aspect ratio (*Str*), the roughness (*Sa*), the residual stress and the hardness results, were examined from pockets 3 and 4 (as before mentioned in Section 2.3). The average values were calculated from the two measurements

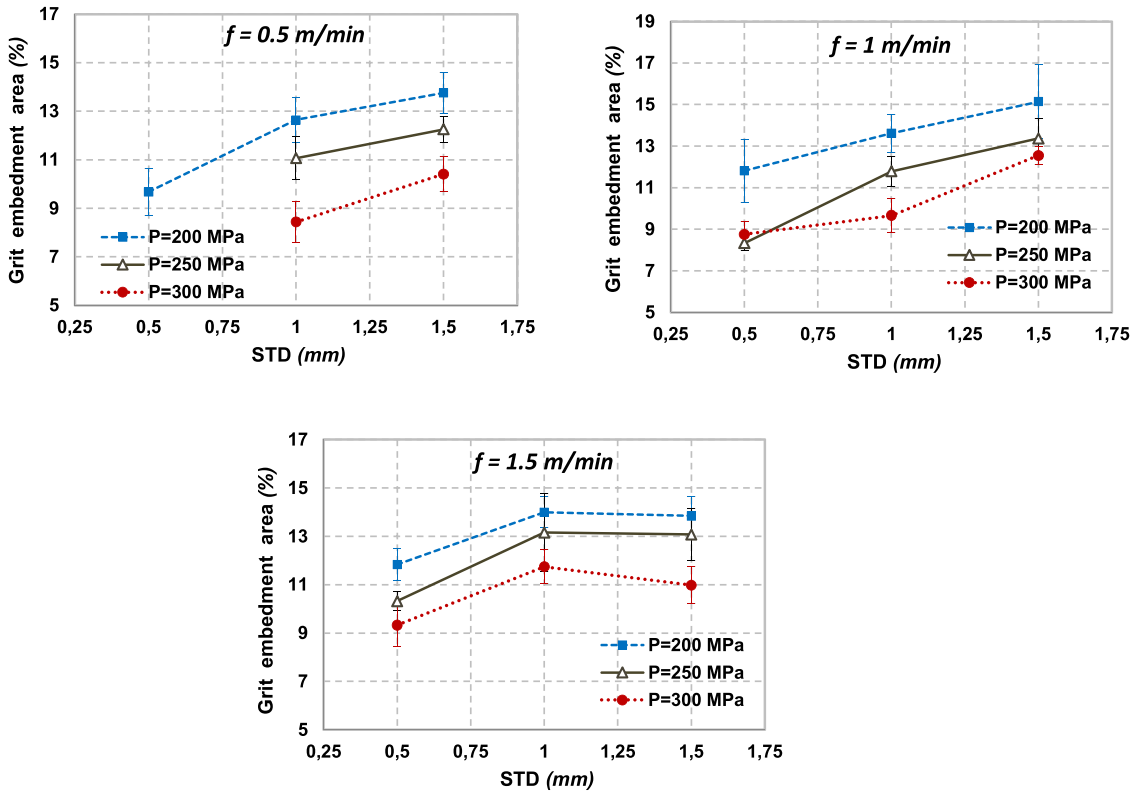

Fig. 13. Effect of the AWJ milling parameters on the grit embedment area in function of step-over distances for various pressures and for a traverse speed of (a) *0.5 m/min*, (b) *1 m/min* and (c) *1.5 m/min*.

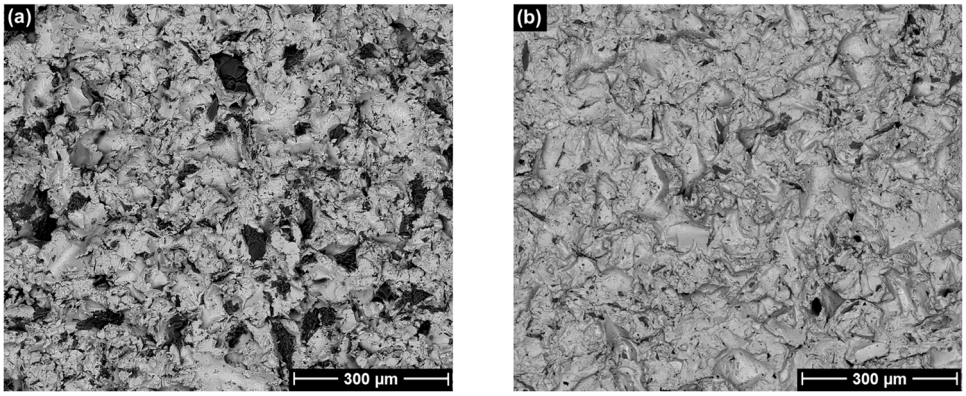

Fig. 14. SEM micrographs of surfaces showing grit embedment in black color (a) before PWJ cleaning (specimen milled by AWJ at $P = 200$ *MPa*, $f = 1.5$ *m/min* and *STD* = *1.0 mm*) and (b) after PWJ cleaning of the same specimen (PWJ cleaning performed at $P = 200$ *MPa*, $f = 1$ *m/min* and *STD* = *0.5 mm*).

performed at the same of parameters with standard deviation.

As shown in Fig. 17, the *Str* parameter (indicator of the degree of surface isotropy) remained almost constant after cleaning of the milled surfaces. This means that the impact of the water droplets on the surface not significantly modify the surface texture produced by the abrasive particles during AWJ milling. This can be observed in 3D surface textures of the milled pockets against the cleaned pockets depicted in Figs. 19–21 . It can be seen that surface topography remains almost the same before and after PWJ cleaning. However, in some specimens, surface texture slightly decreases (Fig. 21**a–b**) or increases (Fig. 20**a–b**). At the same time, when comparing the surface roughness (obtained in previous work [20]) before and after PWJ process, it is revealed that the roughness values are slightly increased after PWJ cleaning (Fig. 18). The increase in roughness or in texture after PWJ cleaning is probably due to the fact that the dislodging of the abrasive particles leads to additional craters. The case of decrease in surface texture is due to water droplets could slightly smooth the peaks produced by AWJ milling. It could be also noteworthy that even the texture-aspect ratio (*Str*) was almost identical before and after PWJ cleaning, *Sal* parameter would be relevant for milled surfaces as it is related to the *STD* process parameter (Fig. 12**)**; *Sal* values should decrease as *STD* decreases (Figs. 19–21**)**. As well as, the developed area *Sdr*, give additional information regarding the surface complexity, especially when comparing several stages of processing [24] as in the case of AWJ milling followed by PWJ cleaning process.

As expected, features become more refined as the *Sal* values decreases, however, *Sal* values not necessarily resulted in higher values for larger *STD*, indicating greater complexity of surfaces, better described by the hybrid parameter *Sdr*. Smoother surfaces have smaller percentage of *Sdr* (*e.g.* Fig. 21**a**). In all experiments (Figs. 19–21), *Sdr* values resulted

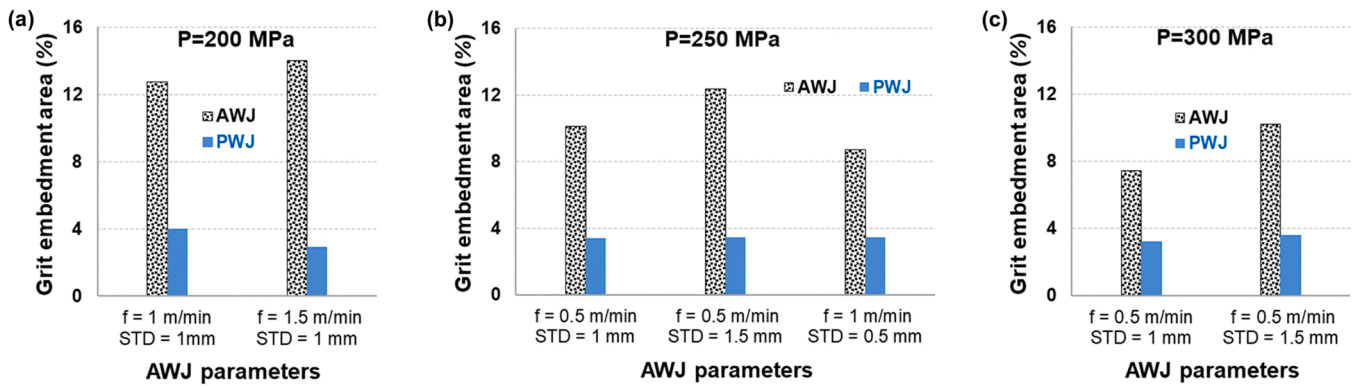

Fig. 15. Surface fraction of grit embedment after AWJ milling and PWJ cleaning for different AWJ process parameters, (a) $P = 200\ MPa$, (b) $P = 250\ MPa$ and (c) $P = 300\ MPa$.

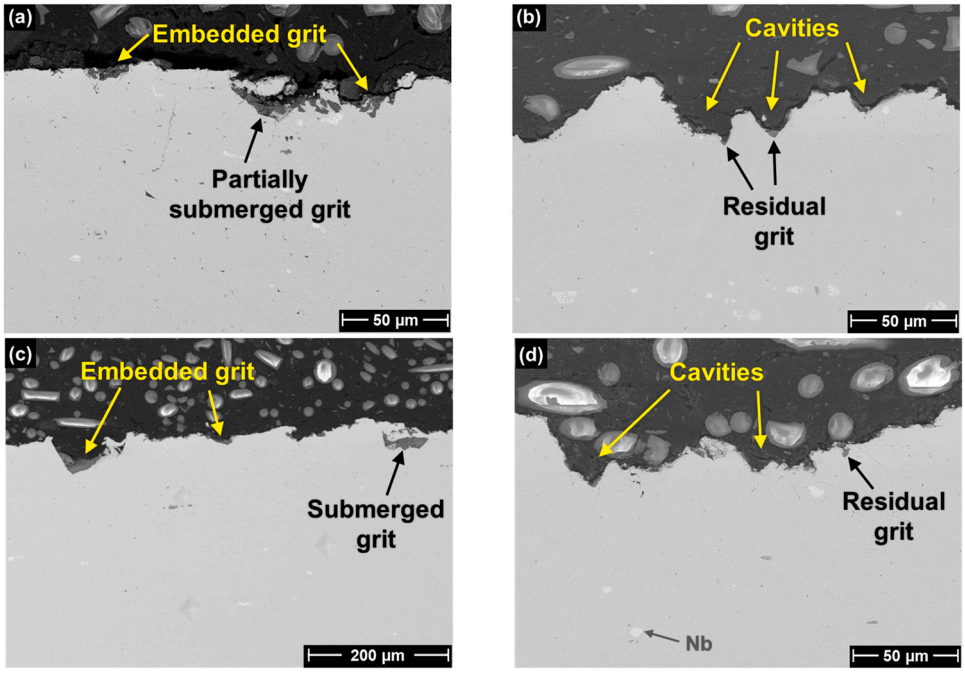

Fig. 16. SEM micrographs (a) in cross-section perpendicular to feed direction of the specimen milled by AWJ at $P = 250\ MPa$, $f = 1\ m/min$ and $STD = 0.5\ mm$, and (b) in cross-section parallel to feed direction of the same specimen after PWJ cleaning; (c) in-cross section parallel to feed direction of the specimen milled by AWJ at $P = 300\ MPa$, $f = 0.5\ m/min$ and $STD = 1.5\ mm$, (d) in cross-section perpendicular to feed direction of the same specimen after cleaned by PWJ.

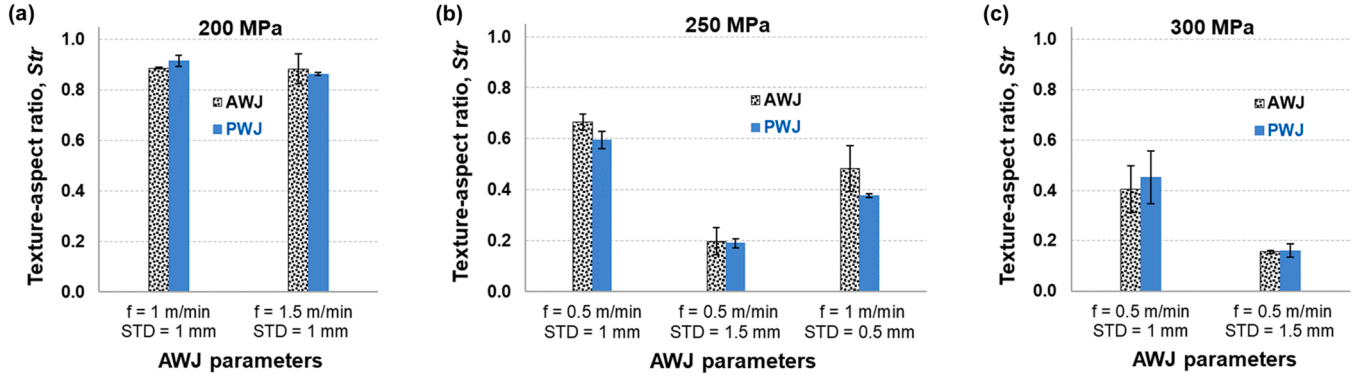

Fig. 17. Surface texture after AWJ milling and PWJ cleaning for different AWJ process parameters, (a) $P = 200\ MPa$, (b) $P = 250\ MPa$ and (c) $P = 300\ MPa$.

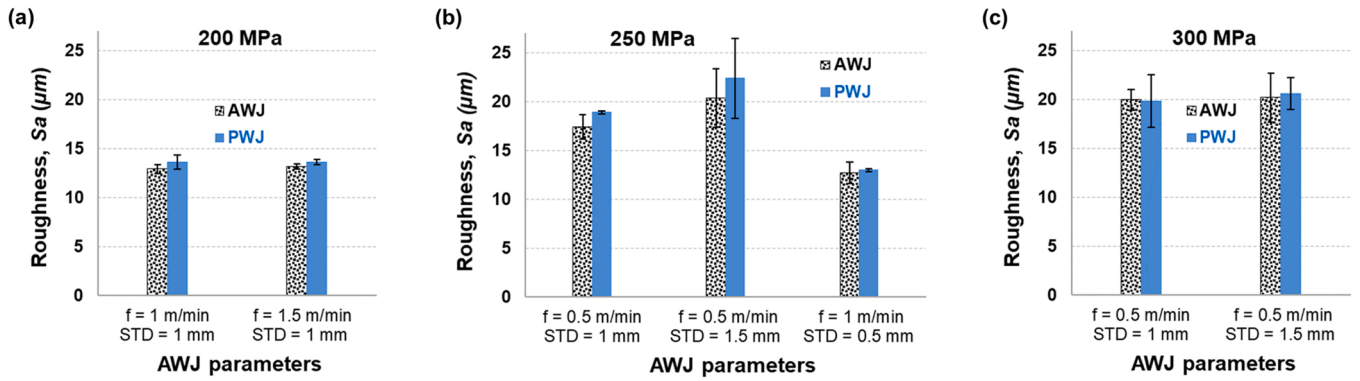

Fig. 18. Surface roughness after AWJ milling [20] and PWJ cleaning for different AWJ process parameters, (a) $P = 200\ MPa$, (b) $P = 250\ MPa$ and (c) $P = 300\ MPa$.

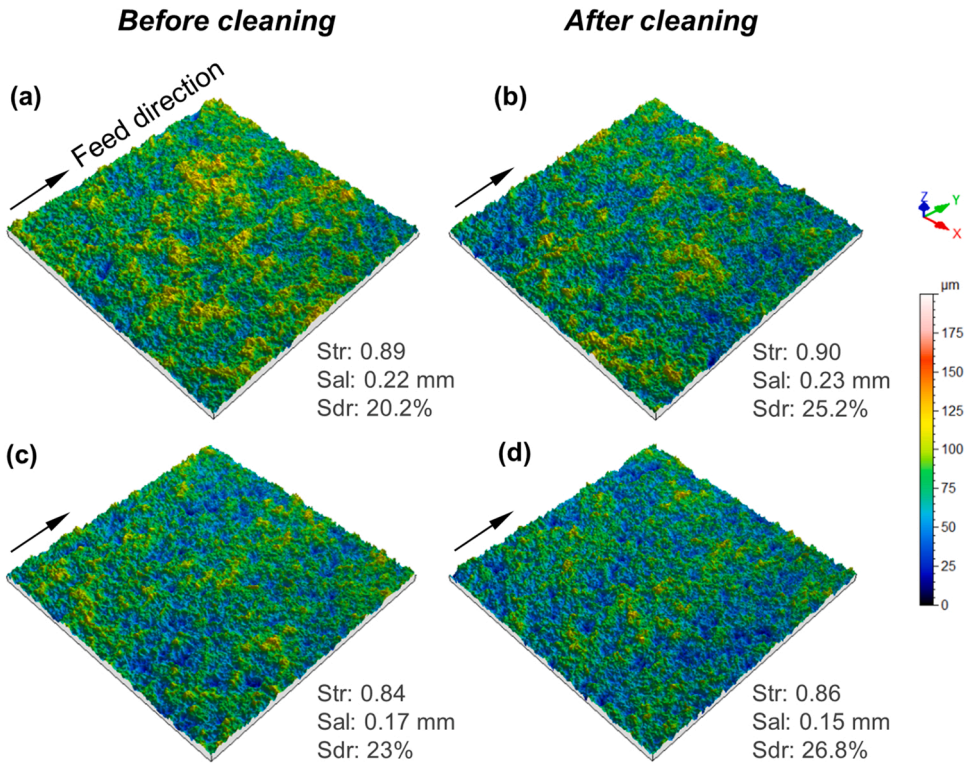

Fig. 19. Different IN718 surface textures (a) after AWJ milling at $P = 200\ MPa$, $f = 1\ m/min$ and $STD = 1\ mm$ and (b) after PWJ cleaning of the same specimen; (c) after AWJ milling at $P = 200\ MPa$, $f = 1.5\ m/min$ and $STD = 1\ mm$ and (d) after PWJ cleaning of the same specimen. (PWJ cleaning at $P = 200\ MPa$, $f = 1\ m/min$ and $STD = 0.5\ mm$). The little arrow indicates the feed direction. Surfaces are $5\ mm \times 5\ mm$ in size.

smaller before than after PWJ cleaning, suggesting the interaction of different stages of processing, between the features initially produced by milling at a certain set of process parameters on which other smoother features were induced by different PWJ cleaning process parameters.

Fig. 22 represents the effect of the PWJ process on the erosion depth on specimens obtained by different conditions of machining of the AWJ (previously published [20]). It is clear form these graphs, the eroded depth remains constant after cleaning operation conducted by the PWJ.

Microhardness measurements were conducted on two specimens before and after PWJ cleaning. A hardness gradient of about 30 % with respect to the bulk material is observed at about $40\ \mu m$ beneath the surface with a return to bulk values ($\sim 245 \pm 15\ HV$) at about $200\ \mu m$ in depth (Fig. 23). Comparable microhardness values and gradients were measured in uncleaned and cleaned surfaces. This confirms that the plastic deformation of the surface layer is due to the abrasive particle impacts during AWJ milling, and that PWJ cleaning operation has not relieve surface stresses, since water droplets have not almost removed material. This can be verified when comparing compressive residual stress results before and after cleaning (Fig. 24). It is consistent that an increase in hardening co-exists with high compressive residual stresses at surface. Further, it is also observed that the level/extent of plastic deformation is depending on the kinetic energy and the exposure time of the jet. This explains that higher plastic deformation was induced by AWJ milling in the specimen milled at $P = 300\ MPa$ (Fig. 23b) than that milled at $P = 250\ MPa$ (Fig. 23a) (*i.e.* $333 \pm 29\ HV$ and $310 \pm 8\ HV$ respectively near to the surface).

Residual stresses after AWJ milling and PWJ cleaning show a compressive residual stress state at surface (Fig. 24) which is beneficial for fatigue life components [14]. These compressive residual stresses after PWJ cleaning seem to be slightly reduced in both *xx* and *yy* directions overall the tests. Such reduction ranges between *30 MPa* and *100 MPa* depending on the AWJ milling parameters. This is probably due to two facts: (1) the dislodging of embedded particles leads to a relief of residual stresses and (2) because of the removal from the upper

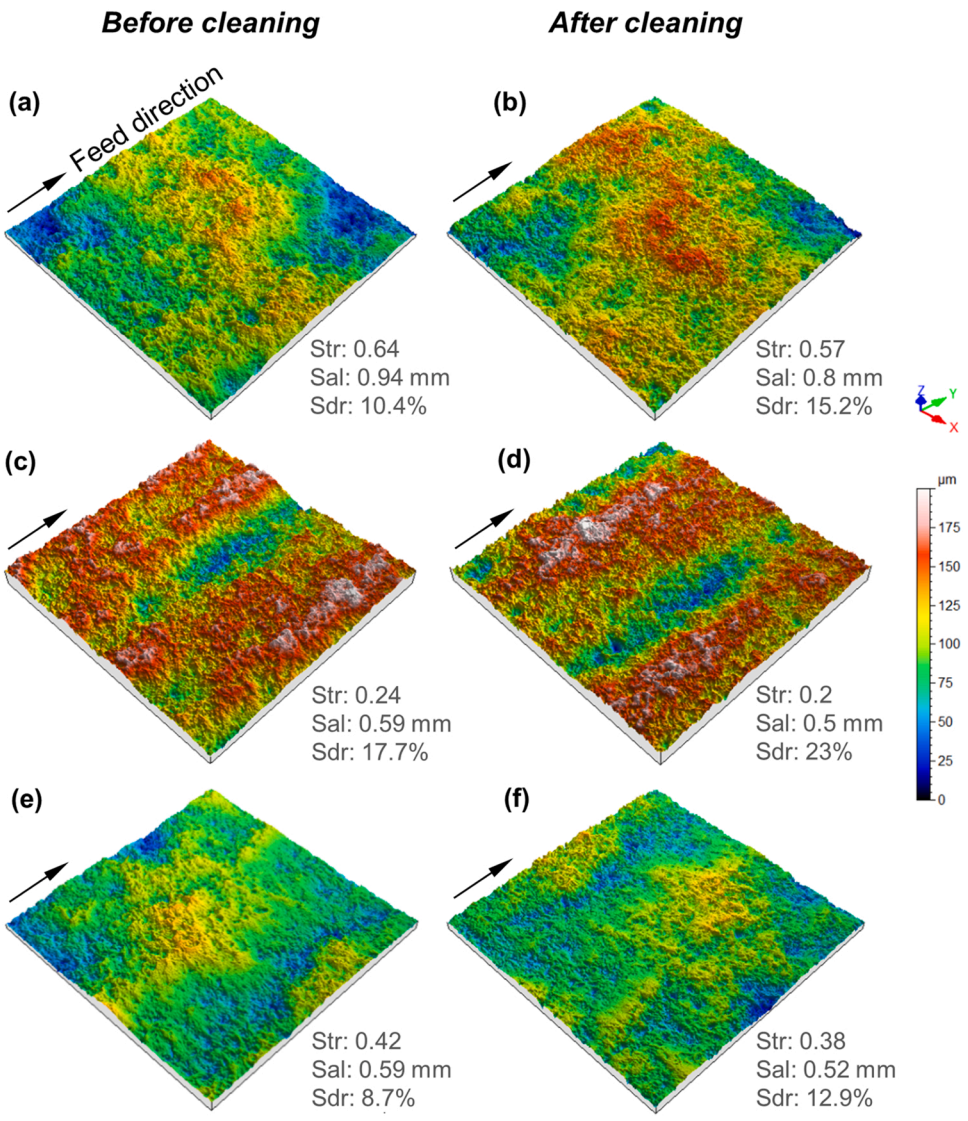

Fig. 20. Different IN718 surface textures (a) after AWJ milling at $P = 250\ MPa$, $f = 0.5\ m/min$ and $STD = 1\ mm$ and (b) after PWJ cleaning of the same specimen; (c) after AWJ milling at $P = 250\ MPa$, $f = 0.5\ m/min$ and $STD = 1.5\ mm$ and (d) after PWJ cleaning of the same specimen; (e) after AWJ milling at $P = 250\ MPa$, $f = 1\ m/min$ and $STD = 0.5\ mm$ and (f) after PWJ cleaning of the same specimen. (PWJ cleaning at $P = 200\ MPa$, $f = 1\ m/min$ and $STD = 0.5\ mm$). The little arrow indicates the feed direction. Surfaces are $5\ mm \times 5\ mm$ in size.

surface layer material which retained stresses. Muruganandhan et al. [29] reported no significant changes in compressive residual stresses values after PWJ in aluminum alloy, affirming that this is due to the effect of the surface erosion. For improving compressive residual stresses, the process parameters should generate significant deformation in surface and subsurface region.

Further, it can be noticed that when milling, the jet produced slightly higher residual stresses in feed direction (*yy*) compared with those initially measured in the bulk material. However, even when difference between σxx and σ_{yy} of the wrought IN718 material was *200 MPa* due to the effect of rolling manufacturing, this residual stress state becomes more isotropic after AWJ milling.

4. Conclusions

The impact of PWJ cleaning operation was experimentally analyzed on Inconel 718 surfaces prior milled by AWJ process. Firstly, the influence of AWJ parameters (*viz.* water pressure, traverse speed and step-over distance) were analyzed on the degree of abrasive embedment and the surface texture. Then, the effectiveness of PWJ to remove the embedded grit with the minimal thickness loss and the minimal modification in surface state after cleaning were evaluated. For the experimental conditions investigated in this study, the following conclusions can be highlighted:

- Before PWJ cleaning, all surfaces presented embedded abrasive particles which surface fraction varied from 7 % to 15 % depending on the AWJ milling conditions. The grit embedment decreases when increasing the pressure but decreasing the step-over distance.
- PWJ cleaning considerably reduced the fraction of embedded grit on the AWJ milled surfaces by up to 80 % of the total fraction. Residual abrasives fraction of ~ 4 % remained in all cleaned surfaces regardless of the initial level of grit embedment obtained from the different process parameters used for AWJ milling, meaning that, from micrographs observations, the 4 % of remaining grit is mostly submerged particles that could not be dislodged by PWJ cleaning.
- Surface topography was characterized by a set of parameters: *Sa*, *Str*, *Sal* and *Sdr*. PWJ cleaning neither induced major material loss (between *2* and *100* μm) nor significant modification in the surface texture and roughness because the water droplets have almost not eroded the material surface state produced by abrasive particles. These slight modifications in surface topography were attributed to the dislodge of the abrasive grit and/or the different process parameters used for AWJ milling and PWJ cleaning.
- PWJ cleaning was not modified the surface hardening produced by AWJ milling because water droplets have not significantly eroded

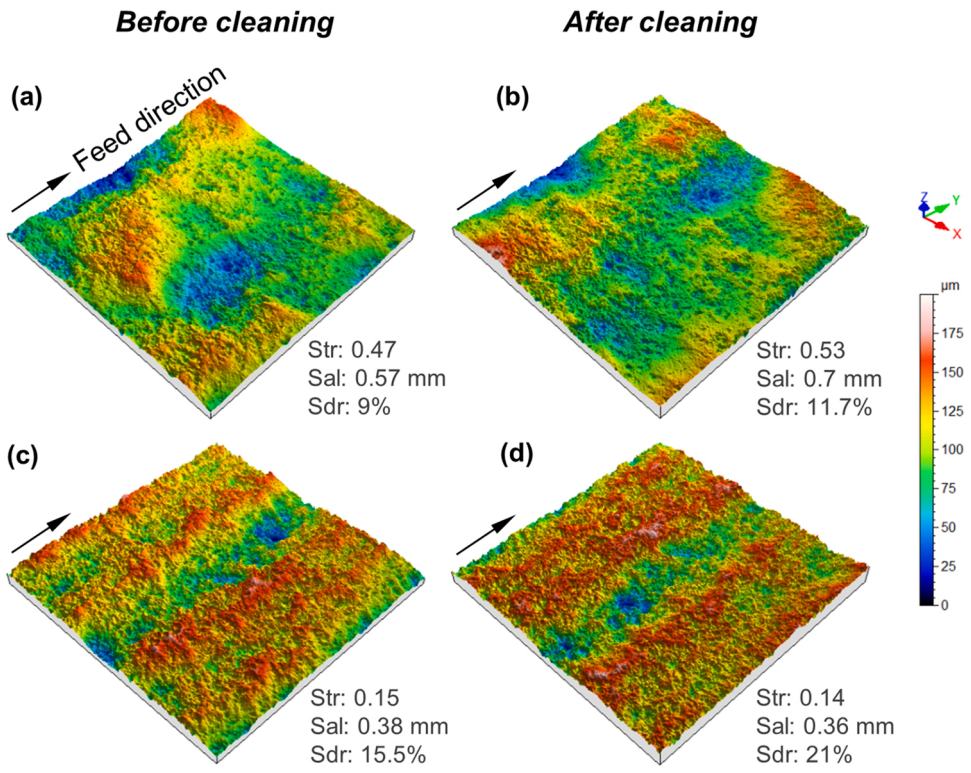

Fig. 21. Different IN718 surface textures (a) after AWJ milling at $P = 300\ MPa$, $f = 0.5\ m/min$ and $STD = 1\ mm$ and (b) after PWJ cleaning of the same specimen; (c) after AWJ milling at $P = 300\ MPa$, $f = 0.5\ m/min$ and $STD = 1.5\ mm$ and (d) after PWJ cleaning of the same specimen. (PWJ cleaning at $P = 200\ MPa$, $f = 1\ m/min$ and $STD = 0.5\ mm$). The little arrow indicates the feed direction. Surfaces are $5\ mm \times 5\ mm$ in size.

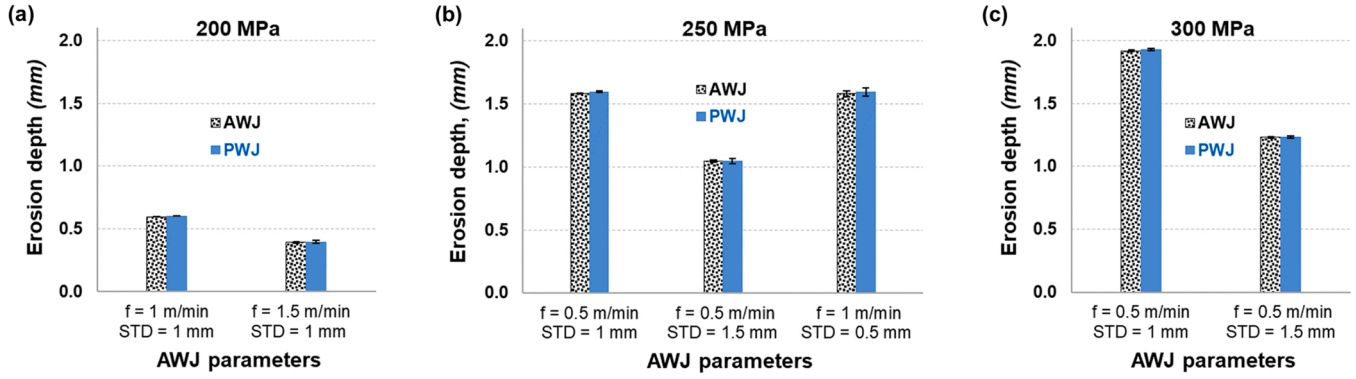

Fig. 22. Material erosion thickness after AWJ milling [20] followed by PWJ cleaning for specimens milled at different process parameters, (a) $P = 200\ MPa$, (b) $P = 250\ MPa$, (c) $P = 300\ MPa$. (The thickness of bulk plate material was $3.71\ mm$ before AWJ milling).

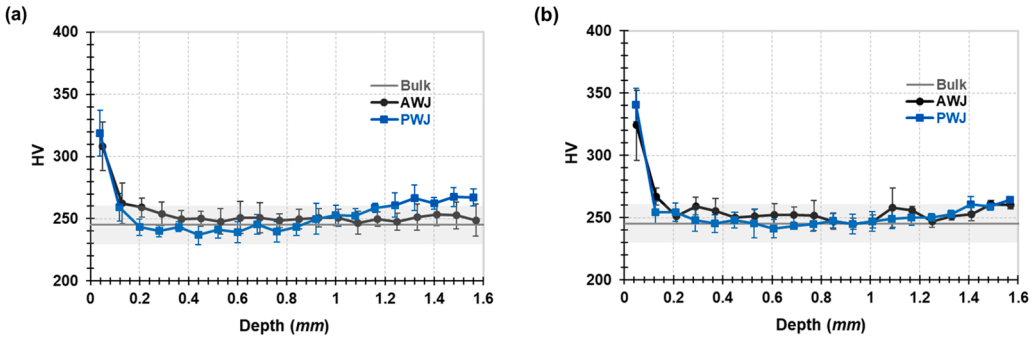

Fig. 23. Microhardness values as a function of the distance to the processed surfaces towards core material before and after PWJ cleaning of the specimens milled at (a) $P = 250\ MPa$, $f = 1\ m/min$, $STD = 0.5\ mm$, and (b) $P = 300\ MPa$, $f = 0.5\ m/min$, $STD = 1.5\ mm$.

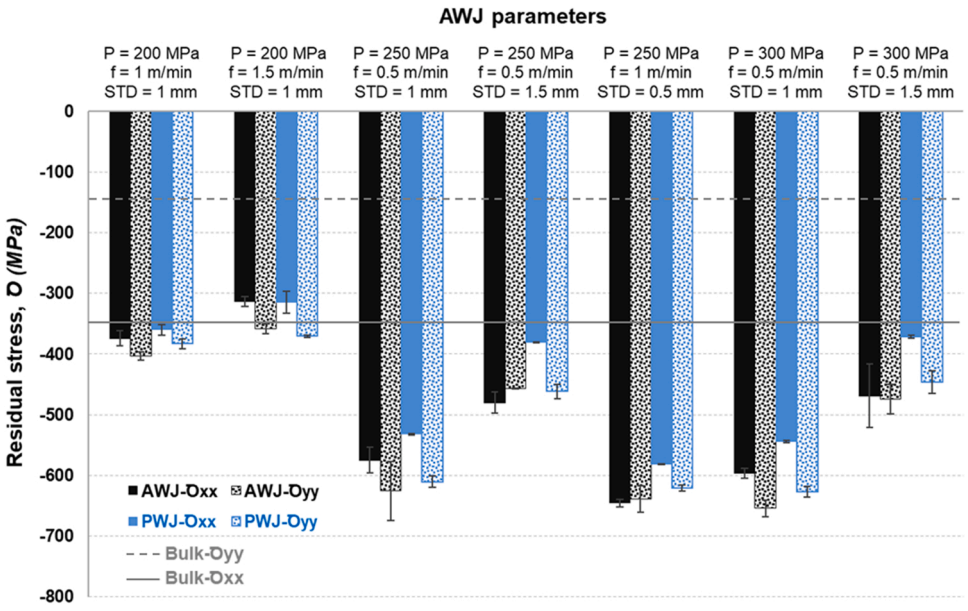

Fig. 24. Residual stresses at surface after AWJ milling [20] and PWJ cleaning for different specimens. (The solid and dotted gray lines indicate the magnitude of residual stresses measured on IN718 surfaces in initial wrought state).

the material. Hence, taking into account the standard deviations, similar values (~ *250 HV*) and gradients of microhardness were observed before and after PWJ cleaning with a peak of hardening at surface corresponding to 30 % higher than that of the bulk.

- The hardening is associated with compressive residual stresses which were produced by AWJ milling and were not considerably affected by PWJ cleaning (between *30* and *100 MPa* of reduction), ranging from − *300* to − *650 MPa* after PWJ cleaning, depending on the AWJ process parameters.

Thus, the present research allowed a thorough analysis of the surface state condition induced by the PWJ post-process applied after AWJ milling, such combination of processes is an interesting alternative for milling difficult-to-machine materials as IN718, as well as, for a repair application where is necessary to remove the damage zone of aeroengine components. Nevertheless, the principal disadvantage of AWJ milling is the grit embedment. High levels of embedded grit may induce fatigue failure for finished surfaces or be a detrimental condition for an intermediate stage. In such cases, PWJ cleaning proved to be an effective and economical post-processing after AWJ milling because it uses the same system without abrasive.

Declaration of Competing Interest

The authors declare that they have no known competing financial interests or personal relationships that could have appeared to influence the work reported in this paper.

Data Availability

Data will be made available on request.

Acknowledgments

The authors gratefully acknowledge the financial support of CONACYT Mexico. The technical support of Karine Vieillevigne [b] is also thank.

References

[1] Momber AW, Kovacevic R. Principles of abrasive water jet machining. London: Springer London; 1998. https://doi.org/10.1007/978-1-4471-1572-4.
[2] Kong MC, Axinte D, Voice W. An innovative method to perform maskless plain waterjet milling for pocket generation: a case study in Ti-based superalloys. Int J Mach Tools Manuf 2011;51(7–8):642–8. https://doi.org/10.1016/j.ijmachtools.2011.04.006.
[3] Rivero A, Alberdi A, Artaza T, Mendia L, Lamikiz A. Surface properties and fatigue failure analysis of alloy 718 surfaces milled by abrasive and plain waterjet. Int J Adv Manuf Technol 2018;94(5):2929–38. https://doi.org/10.1007/s00170-017-0979-5.
[4] Boud F, Carpenter C, Folkes J, Shipway PH. Abrasive waterjet cutting of a titanium alloy: the influence of abrasive morphology and mechanical properties on workpiece grit embedment and cut quality. J Mater Process Technol 2010;210(15):2197–205. https://doi.org/10.1016/j.jmatprotec.2010.08.006.
[5] Fowler G, Shipway PH, Pashby IR. A technical note on grit embedment following abrasive water-jet milling of a titanium alloy. J Mater Process Technol 2005;159(3):356–68. https://doi.org/10.1016/j.jmatprotec.2004.05.024.
[6] Shipway PH, Fowler G, Pashby IR. Characteristics of the surface of a titanium alloy following milling with abrasive waterjets. Wear 2005;258(1):123–32. https://doi.org/10.1016/j.wear.2004.04.005.
[7] Arola D, McCain ML, Kunaporn S, Ramulu M. Waterjet and abrasive waterjet surface treatment of titanium: a comparison of surface texture and residual stress. Wear 2001;249(10):943–50. https://doi.org/10.1016/S0043-1648(01)00826-2.
[8] Singh J, Jain SC. Mechanical issues in laser and abrasive water jet cutting. JOM 1995;47(1):28–30. https://doi.org/10.1007/BF03221126.
[9] Bremer C, Automated repair and overhaul of aero-engine and industrial gas turbine components. Presented at the ASME turbo expo 2005: power for land, sea, and air; 2008, p. 841–6. ⟨https://doi.org/10.1115/GT2005-68193⟩.
[10] Sourd X, Zitoune R, Hejjaji A, Salem M, Hor A, Lamouche D. Plain water jet cleaning of titanium alloy after abrasive water jet milling: surface contamination and quality analysis in the context of maintenance. Wear 2021;477:203833. https://doi.org/10.1016/j.wear.2021.203833.
[11] Patel KJ. Quantitative evaluation of abrasive contamination in ductile material during abrasive water jet machining and minimising with a nozzle head oscillation technique. Int J Mach Tools Manuf 2004;44(10):1125–32. https://doi.org/10.1016/j.ijmachtools.2003.12.007.
[12] Donachie MJ, Donachie SJ. Cleaning and finishing. In: Superalloys: a technical guide. 2nd ed. Materials Park, OH: ASM International; 2002. p. 203–10.
[13] Awad SB, Nagarajan R. Ultrasonic cleaning. In: Kholi R, Mittal KL, editors. Developments in surface contamination and cleaning. Norwich, NY, U.S.A: W. Andrew Pub; 2008. p. 225–80.
[14] Lieblich M, et al. On the fatigue behavior of medical Ti6Al4V roughened by grit blasting and abrasiveless waterjet peening. J Mech Behav Biomed Mater 2016;63:390–8. https://doi.org/10.1016/j.jmbbm.2016.07.011.
[15] Huang L, Kinnell P, Shipway PH. Parametric effects on grit embedment and surface morphology in an innovative hybrid waterjet cleaning process for alpha case removal from titanium alloys. Procedia CIRP 2013;6:594–9. https://doi.org/10.1016/j.procir.2013.03.077.

[16] Arola D, Alade AE, Weber W. Improving fatigue strength of metals using abrasive waterjet peening. Mach Sci Technol 2006;10(2):197–218. https://doi.org/10.1080/10910340600710105.
[17] Azhari A, Schindler C, Godard C, Gibmeier J, Kerscher E. Effect of multiple passes treatment in waterjet peening on fatigue performance. Appl Surf Sci 2016;388:468–74. https://doi.org/10.1016/j.apsusc.2015.11.195.
[18] Huang L, Kinnell P, Shipway PH. Removal of heat-formed coating from a titanium alloy using high pressure waterjet: influence of machining parameters on surface texture and residual stress. J Mater Process Technol 2015;223:129–38. https://doi.org/10.1016/j.jmatprotec.2015.03.053.
[19] Holmberg J, Wretland A, Berglund J, Beno T. Surface integrity after post processing of EDM processed Inconel 718 shaft. Int J Adv Manuf Technol 2018;95(5):2325–37. https://doi.org/10.1007/s00170-017-1342-6.
[20] Cano-Salinas L, Moussaoui K, Hejjaji A, Salem M, Hor A, Zitoune R. Influence of abrasive water jet parameters on the surface integrity of Inconel 718. Int J Adv Manuf Technol 2021;114(3):997–1009. https://doi.org/10.1007/s00170-021-06888-9.
[21] Avegnon KLM, Schmitter DC, Meisman S, Hadidi H, Vieille B, Sealy MP. Areal surface texture and tool wear analysis from machining during powder bed fusion. Procedia CIRP 2022;108:704–9. https://doi.org/10.1016/j.procir.2022.03.109.
[22] Pawlus P, Reizer R, Wieczorowski M, Krolczyk G. Parametric description of one-process surface texture. In: Proceedings of the 2021 6th international conference on nanotechnology for instrumentation and measurement (NanofIM); 2021, p. 1–4. ⟨https://doi.org/10.1109/NanofIM54124.2021.9737339⟩.
[23] Fu S, Cheng F, Tjahjowidodo T. Surface topography measurement of mirror-finished surfaces using fringe-patterned illumination. Metals 2020;10(1):69. https://doi.org/10.3390/met10010069.
[24] Leach R (Ed.), Characterisation of areal surface texture. Berlin, Heidelberg: Springer Berlin Heidelberg; 2013. ⟨https://doi.org/10.1007/978-3-642-36458-7⟩.
[25] Fowler G, Pashby IR, Shipway PH. The effect of particle hardness and shape when abrasive water jet milling titanium alloy Ti6Al4V. Wear 2009;266(7):613–20. https://doi.org/10.1016/j.wear.2008.06.013.
[26] Hejjaji A, Zitoune R, Toubal L, Crouzeix L, Collombet F. Influence of controlled depth abrasive water jet milling on the fatigue behavior of carbon/epoxy composites. Compos Part A: Appl Sci Manuf 2019;121:397–410. https://doi.org/10.1016/j.compositesa.2019.03.045.
[27] Getu H, Spelt JK, Papini M. Conditions leading to the embedding of angular and spherical particles during the solid particle erosion of polymers. Wear 2012;292–293:159–68. https://doi.org/10.1016/j.wear.2012.05.017.
[28] Hadavi V, Arani NH, Papini M. Numerical and experimental investigations of particle embedment during the incubation period in the solid particle erosion of ductile materials. Tribol Int 2019;129:38–45. https://doi.org/10.1016/j.triboint.2018.08.013.
[29] Muruganandhan R, Mugilvalavan M, Thirumavalavan K, Yuvaraj N. Investigation of water jet peening process parameters on AL6061-T6. Surf Eng 2018;34(4):330–40. https://doi.org/10.1080/02670844.2017.1394564.